Scanning Electron Microscopy

Volume 1985
Number 1 *1985*

Article 4

11-26-1984

Sputtered Thermal Ion Mass Spectrometry as a New Quantitative Method for In-Depth Analysis

G. Blaise
University of Paris

SCANNING ELECTRON MICROSCOPY/1985/I (Pages 31-42)
SEM Inc., AMF O'Hare (Chicago), IL 60666 USA

0586-5581/85$1.00+.05

SPUTTERED THERMAL ION MASS SPECTROMETRY AS A NEW QUANTITATIVE METHOD FOR IN-DEPTH ANALYSIS

G. Blaise

Laboratoire de Physique des Solides, Université Paris-Sud
Bâtiment 510 - 91405 Orsay Cédex (France)
Phone No.: (6) 941-53.60

(Paper received April 15 1984, Completed manuscript received November 26 1984)

Abstract

The Sputtered Thermal Ion Mass Spectrometry method (STIMS) consists of collecting a part of the matter sputtered from a solid by ion bombardment into a heated cell where it is reduced into atoms. A thermal ionization process or an electron impact process taking place in the cell yields ions which are extracted and mass analyzed. The composition of the solid is determined from ion intensities after calibration of ionization coefficients. It has been demonstrated that the method has an absolute quantitative character. Applications to elemental quantitative analysis (identification of new compounds in diffusion couples, dust particle analysis) and in-depth analysis of thin layers (unannealed, annealed and amorphous layers) are being developed. We have found that in-depth resolution is better in annealed layers than in unannealed ones, it can be improved by lowering the primary ion energy below 2 keV and it is very good in amorphous materials.

Key words : In depth analysis, Ion Sputtering, Mass Spectrometry, Surface analysis method, Thin layer, Thermal Ionization, Solid quantitative analysis, Diffusion.

Introduction

Since Castaing and Slodzian (Castaing and Slodzian, 1962, Slodzian, 1964) have proposed the first localized analysis method of solid surfaces using the secondary ion emission which results from ion sputtering, many other analytical approaches, also based upon sputtering, have recently been proposed. Among the most attractive, I would mention the sputtered neutral mass spectrometry (SNMS) proposed by Oechsner et al. (1979), the laser probe mass spectrometry (LPMS) developed by Eloy (1980) or the optical spectroscopy and mass spectrometry methods using the glow discharge or the hollow cathode discharge (Marcyk and Streetman, 1976, Harrison and Magee, 1974). These methods share the property of deriving directly the analytical information from the initial state of particles as they are emitted in the sputtering process: ejected atoms and aggregates- neutral, excited or ionized- are used in the mass spectrometry techniques and optical spectroscopy. In all the methods, the sputtering process utilized to sample solids simultaneously conditions more or less the character and intensity of the physical process used for analytical purposes. The most obvious case is the secondary ion emission in which ion species and their intensities are very strongly affected by the nature of elements present in the solid or at the surface and their chemical affinity (Slodzian, 1975, Blaise and Bernheim, 1975). As a result of this, signals depend not only on the composition of the sample, which is the goal looked for, but also on the chemical nature of the matter. We say that we have to do with matrix effects.

In order to eliminate matrix effects it is necessary that the withdrawal of matter and the physical process which allows the chemical identification of elements are independent. This implies a treatment of the sputtered matter. In the glow discharge optical spectroscopy the plasma density seems sufficiently high for the sputtered matter to be close to the plasma temperature. Thus the observed optical spectrum is rather characteristic of the plasma than of sputtering. However, in this case, the treatment is not really complete first because ion bombardment induced light emission still contributes to signal, second because recombinations of the sputtered species in the plasma do not necessarily reflect the sample composition congruously.

The method that Castaing and I have developed involves a thermal treatment of sputtered matter Blaise and Castaing (1977, 1978), Castaing and Blaise (1980). The complexity of this matter is well known, but it turns out that under the stationary sputtering regime, its overall composition is identical to that of the sample. Thus a treatment that "would mill" the matter to reduce it in atomic components would open the way to a quantitative method of analysis. The thermal treatment consists of collecting a part of the sputtered matter in a cell brought at a very high temperature where it remains for a sufficiently long time to be thermalized. Then analysis is performed by extracting from the cell ionized atoms that one determines by mass spectrometry. The association of sputtering and thermalization leads us to baptize this method "Sputtered Thermal Ion Mass Spectrometry" (STIMS). This is essentially a quantitative method for characterizing the elemental composition of solid samples.

Solid surface analysis evidently is not limited to determining the sample elemental composition- electron spectroscopy and secondary ion emission are rich in informations of all kinds- but now we, too often, neglect the advantage of an elemental composition analysis which in a way constitutes the stumbling-block of the knowledge of so complex a structure as a surface.

Having described the method and presented its main features we will present a certain number of its applications for quantitative elemental analysis and in-depth analysis of thin layers.

The sputtered thermal ion mass spectrometry method. Blaise and Castaing (1978), Castaing and Blaise (1980).

A fraction of sputtered particles is collected in a heated cell through the opening O' under a solid angle $\Delta\Omega$ (see Fig. 1). The cell is made of a refractory metal (tantalum or tungsten) and is heated to a high temperature ($\sim$ 3000 K). In the course of their collisions on the cell wall molecular aggregates are progressively dissociated into their atomic components and a proportion of them is ionized,either by a thermal-ionization process at the cell wall or by electron impact using a filament-cell diode device which will be described further. Ions produced in one of these modes are extracted by an external electric field through another aperture O opposite to O'. The ion beam is then conveniently focused by an appropriate ion-optical system (L_1, L_2 on Fig. 2) onto the entrance slit of a mass spectrometer. Opening O' is set off the optical axis in order to prevent a direct passing of secondary ions sputtered from the sample through the cell. A multidetection system composed of channeltrons is used which can be moved along the exit face of the magnet. They are fixed at appropriate positions to collect particular elements simultaneously. Signals are integrated over one second of time and stored in a computer. A program allows to calculate concentrations and to plot them as a function of depth in in-depth applications, as the experiment proceeds.

Characteristics of the heated cell.

Collection of sputtered particles : In order to keep the composition of the sputtered material entering the cell unchanged, it is essential that no discrimination among the sputtered species takes place in the collection angle $\Delta\Omega$. In the first place, this requires a field free region between the sample and the heated chamber in order to collect ions of any charge. Secondly the same emission anisotropy for the various molecular species is necessary. Earlier studies of a copper-aluminium alloy found the Al to Cu concentration ratio to be independent of the emergence angle (Tarento, 1982). From this, it is concluded that the emission anisotropy is about the same for the two species.

The number of atoms n injected into the cell per second is given by (Fig. 1) :

$$n = N_p \frac{S(\theta)}{\pi} \Delta\Omega \cos\alpha \qquad (1)$$

where N_p is the number of primary ions impinging on the sample per second, $S(\theta)$ the sputtering yield at θ incidence angle, α the collection angle to the surface normal and $\Delta\Omega$ the collection solid angle. For a monoatomic solid bombarded at a few keV energy by a primary beam of a few μA, the flux of incoming particles is $n \gtrsim 10^{11}$ at/sec with $\theta = 45°$, $\alpha = \pi/2 - \theta$ and $\Delta\Omega = 2.10^{-3}$srd. If the sample contains an element A at concentration C_A the flux of incoming A atoms will be :

$$n_A = n\, C_A. \qquad (2)$$

Thermalization : The role of the cell is to ensure the thermalization of sputtered matter which consists of the dissociation of aggregates, elimination of secondary ions and slowing down of sputtered particles to thermal velocities.

Let d be the diameter of openings O and O' and D that of the cell supposed to be spherical. The average number of collisions on the walls of a particle before its coming out will be $2(D/d)^2$, that is about a hundred collisions for D $\gtrsim$ 10 mm and d $\gtrsim$ 1 mm. This is probably sufficient for a good thermalization. A recent work (Hennequin and Couchouron, 1979, Couchouron, 1983) dealing with the accommodation of sputtered particles with a hot metal surface has shown that, in fact, most of them seem to be thermalized after a single collision.

When the cell is supplied under the permanent sputtering regime, the atomic volume density of the matter n_g is given by :

$$n_g = \frac{n}{s_0 + s_{0'}} \left(\frac{2\pi m}{kT}\right)^{1/2} \qquad (3)$$

For openings $s_0 \gtrsim s_{0'} \gtrsim 1$ mm^2, $n \gtrsim 10^{11}$at/sec we get $n_g \gtrsim 2.10^{-3}$at/cm^3 at T = 3000 K ; that is an equivalent pressure $P_g \gtrsim 10^{-7}$ torr. Let us notice that at the same temperature the vapor pressure of the cell wall is $\gtrsim 10^{-4}$ torr.

If τ is the resident time of a particle on the cell wall, the density of the adsorbed phase n_{ad} is expressed as :

Figure 1

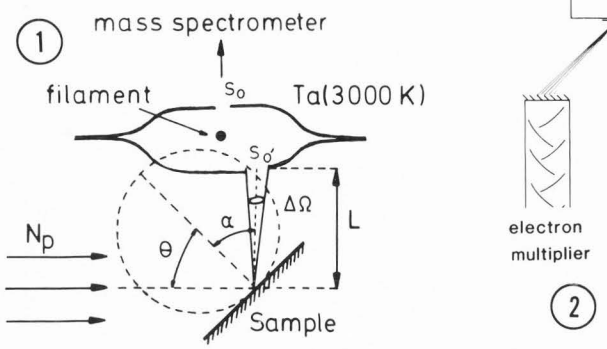

Collection efficiency of the sputtered products into the tantalum cell. Primary ions $N_p \sim 10^{13}$ ion/mm² ; $\theta = \alpha = 45°$; $\Delta\Omega = 2.10^{-3}$ srd ; $s_o \sim s_o' \sim 1$ mm². Diameter of the filament $\phi = 0.3$ mm. Dimensions of the cell = 8 mm height, 12 mm long and 8 mm wide.

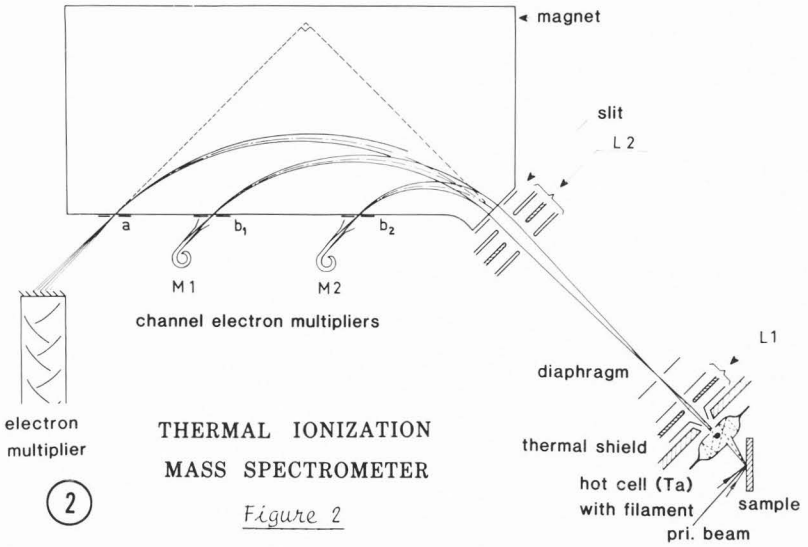

THERMAL IONIZATION MASS SPECTROMETER

Figure 2

Schematic view of the sputtered thermal ion mass spectrometer. Channeltrons M_1 and M_2 are moving along the magnet. The dinode electron multiplier is at a fixed position. It is used for measuring very intense currents like the thermal ionization current of the cell wall which allows the control of the temperature.

$$n_{ad} = \tau \frac{n}{s_0 + s_{0'}} \qquad (4)$$

For $\tau \sim 10^{-3}$s we find $n_{ad} \lesssim 5.10^9$ at/cm² which is very small compared to the atomic surface density of the cell wall $\lesssim 3.10^{14}$ at/cm². Therefore the coverage of the cell wall with sputtered atoms will be extremely low if the resident time is short enough. This condition will be generally fulfilled at high temperature except for some elements exhibiting a very high surface attachment energy.

Assuming thermal equilibrium the molecular dissociation degree calculated at 3000 K reaches 10^7 for molecules with a binding energy $D_0 \lesssim 5$ eV and drops to 0.3 for $D_0 \lesssim 10$ eV. This means that most molecules will be dissociated except those whose binding energy is unusually high.

Ionization : The evolution of the sputtered matter in the cell to thermal equilibrium gives rise to the production of ions in a proportion determined by the Saha-Langmuir equation :

$$\alpha_i^+ \sim \exp - \frac{e(V_i - \phi)}{kT} \qquad (5)$$

where α_i^+ is the ionization coefficient of species i, V_i its ionization potential and ϕ the work function of the cell wall, that is $\phi = 4.10$ V for tantalum. For an element with an ionization potential $V_i \sim 8$ V, the ionization coefficient calculated at 3000 K is about $\alpha_i^+ \sim 10^{-7}$. For a flux of incoming particles $n \sim 10^{11}$ at/sec this leads to a maximum signal of the order of 10^4 c/s. Taking into account the instrumental factors this signal would drop to the detection limit of a few hundred counts/sec. This estimation demonstrates the thermal ionization process becomes inefficient for elements with an ionization potential higher than 8 V. This means that only metal elements with low ionization potential will be detectable. This is a tremendous restriction on the applicability of the method.

A practical utilization of the cell wall vapor thermal ionization as internal thermometer deserves to be mentioned. Combining the temperature dependence of the vapor pressure with the ionization probability we obtain the following expression for the tantalum ion emission as a function of T :

$$I(Ta^+) = AT^{-1} \exp - \frac{\varepsilon_d + e(V_{Ta} - \phi)}{kT} \qquad (6)$$

with the numerical values $V_{Ta} = 7.7$ V, $\phi = 4.15$ V and $\varepsilon_d = 8.15$ eV for the binding energy, we get :

$$I(Ta^+) = 1.7\ 10^{13} T^{-1} \exp - \frac{135652}{T} \qquad (7)$$

Coefficient A has been measured by bringing the cell up to the tantalum melting point (T_m= 3270 K). Using eq. (6) the Ta^+ signal can be used as an internal thermometer whose absolute precision is only about 50 K but whose sensitivity is very high. For example a variation of 10 % of Ta^+ intensity corresponds to 5 K temperature variation. Therefore, by adjusting the tantalum intensity it is possible to reproduce temperature conditions at a few degrees which is essential for the calibration of the thermal ionization coefficients of elements.

The limitation imposed by the thermal ionization process to the detection of elements leads us to look for a complementary ionization means compatible with the thermalization function of the cell. The proposed solution consists of producing an electron impact ionization inside the cell (Blaise et al., 1984). For that a filament is stretched through the cell, facing the exit opening O (Fig. 1, 2). When the filament is negatively biased with respect to the cell wall the emitted electrons are accelerated towards the opening O

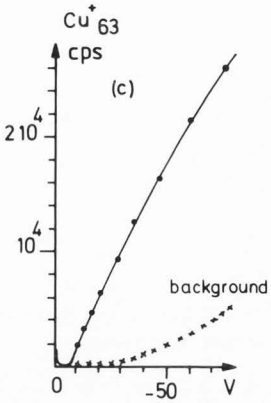

Figure 3

Ionization efficiency of the filament-cell device compared to the thermal ionization process for copper. V = 0 copper thermal ionization yield ∿ 1500 c/s, V ∿ - 8 V lower limit of the copper ionization energy. In this experiment the filament current was 6 mA.

and thereby ionize atoms present in this region. Ions produced are then drained by the external electric field and conveyed to the mass spectrometer. The efficiency of this ionization process is shown in Fig. 3 where we have plotted the Cu^+ signal as a function of the negative filament voltage V. For V = 0 we have a copper thermal ionization signal of about 1500 c/s under the experimental conditions. When V is slightly negative, this signal drops to zero until the electron energy becomes close to the copper ionization energy. Beyond this value the copper signal starts increasing again in proportion as V is becoming more negative. At the same time the background also increases more rapidly than the signal. This background is produced by impurities contained in the cell wall and also components of the residual atmosphere. For V = - 50 V, the copper signal reaches 16000 c/s which is an appreciable gain over the thermal ionization signal and the signal to background ratio is stil large enough to allow a good precision on the measurements.

As the efficiency of electron-impact ionization is not very dependent on the ionization potential, all elements are, in principle, detectable with ion yields of the same magnitude. With the device in present use, the useful yield, including the mass spectrometer transmission and the detector quantum yield, is about 10^{-6}. This leads to signals of the order of 10^5 c/s for pure elements.

Analytical procedure.

Quantitative aspect : Whether the ionization process is thermal or electronic, the ion intensity ratio of two elements A and B is expressed proportionally to their respective concentration ratio as :

$$I(A^+)/I(B^+) = k_{AB} C_A/C_B \qquad (8)$$

where k_{AB} is the relative ionization coefficient measured from standards.

The absolute quantitative character of the method has been demonstrated by showing that k_{AB} is specific for elements A and B, and independent of the compound in which they were embedded. The procedure we used for that consists of measuring k_{AB} on a cyclic sequence of compounds containing A-B ; B-C ; ... X-A. If analysis is quantitative we should get $k_{AB} \cdot k_{BC} \cdot k_{CD} \cdots k_{XA} = 1$. In the two examples given in table 1, one obtains 1.07 and 0.98 for the product of coefficients, using respectively thermal ionization or electron impact ionization. These values are compatible with the precision of 5 % of the measurement of each coefficient.

TABLE 1

Relative ionization coefficients : k^{th}_{AB} measured by using thermal ionization ; k_{AB} measured by using electron impact.

	Al-Cu	Cu-Mg	Mg-Al	Al-Zn	Zn-Cu
k^{th}_{AB}	468	0.091	0.025		
k_{AB}		1.25	0.205	2.2	1.75

This demonstrates the absolute quantitative character of the method (many applications have confirmed this). This conclusion is particularly important in the case of electron impact ionization because we could fear the electric field produced in the cell by the filament is prejudicial to a quantitative result.

The originality of the electron impact ionization device we have used comes from the fact that ionization still takes place in the cell itself where sputtered products are thermalized. This is why quantitative results are still maintained. This result would not have been obtained by simply ionizing sputtered species coming directly from the sample because of matrix effects related to the presence of secondary ions and molecular species.

From a practical point of view k_{AB} can be measured from any standard containing elements A and B. It is not necessary to use standards whose composition is close to that of the sample as for example in SIMS.

The detection limit, calculated for surface analysis of material sputtered from one or two atomic layers over an extended area of 1 mm^2 is about 0.1 % with 10 % statistical accuracy, using the electron impact ionization device. However, two limitations to the detection of elements should be mentioned. One has first to consider the chemical reactivity of the cell. For some elements the attachment energy is so high that memory effects may become important (e.g. niobium) ; for others, such as oxygen, carbon or boron, these are completely dissolved in the tantalum cell wall, which makes them undetectable. The second limitation is due to the components of the residual atmosphere which are ionized by electron impact. Some major components, such as $N_2^+(28)$, give signals so intense that elements of the same mass, $Si^+(28)$ for example, are not detectable. These two disadvantages could be overcome by using refractory cell materials which are less chemically active than Ta and W and by using the hot chamber in an ultra-high vacuum environment for the heated cell (the residual pressure being now $\sim 10^{-7}$ torr).

In-depth analysis : Despite the improvements to be considered, there is little hope to be able to perform a lateral analysis on the scale of a micron as is possible by SIMS. However, in-depth profiling is possible with the same depth resolution as by SIMS. In our case, in-depth profiling

requires the sample to be laterally homogeneous over a minimum area of a few mm^2. Uniform etching is obtained over the analyzed area by scanning the primary ion beam over several mm^2. Using an ion energy in the range of 2 to 6 keV and an ion current density of about 2 $\mu A/mm^2$, erosion progresses at a rate of a few atomic layers per second. Since signals are integrated over one second of time, this means that each integration is representative of the sample composition over a few atomic layers.

In most profiling methods, intensities -or sometimes concentrations- are plotted as a function of the sputter time. In-depth calibration is then obtained by measuring the depth of the crater. This procedure requires very stable sputtering conditions together with constant sputtering yield during erosion. Except for selected materials such as semi-conductors, this last condition is not often fulfilled (Magee et al, 1982). We propose a procedure that can be adapted to any quantitative method. It consists of plotting concentrations as a function of the mass thickness, that is the amount of sputtered material per unit area (such a procedure is already used in electron probe micro-analysis (Heinrich, 1981)).

Let $Q(A^+)$ be the number of A^+ ions collected during the sputtering of a mass per unit area $\mu(A)$ of the sample. As the method is quantitative we can express the proportionality of these two quantities as :

$$Q(A^+) = T\gamma_A \alpha_A^+ \mu(A) \qquad (9)$$

where T is an instrumental factor independent of the element to be considered, α^+_A the ion yield and γ_A a proportionality factor. Coefficient $\Gamma_A = T\gamma_A \alpha_A^+$ is measured by sputtering a layer of known thickness (evaporated layer for example), only composed of atoms A.

Let us now consider a compound A-B. From eq.(9) the ion charge $\Delta Q(A^+, \Delta t)$ collected during a sputter unit time Δt is related to the corresponding mass thickness $\Delta\mu(A, \Delta t)$ of A by :

$$\Delta Q(A^+, \Delta t) = \Gamma_A \Delta\mu(A, \Delta t) \qquad (10)$$

If $\Delta\mu(A\text{-}B, \Delta t)$ is the mass thickness of the compound and $C_A^{\ddot{}}$ the weight concentration, we get :

$$\Delta\mu(A, \Delta t) = \Delta\mu(A\text{-}B, \Delta t)\ C_A^{\ddot{}} \qquad (11)$$

After a sputter time $n\,\Delta t$, the corresponding mass thickness of the material is given by :

$$\mu(A\text{-}B, n\Delta t) = \sum_{i=1}^{n} \frac{\Delta\mu_i(A, \Delta t)}{C^{\ddot{}}_{A_i}} \qquad (12)$$

The in-depth profiling procedure consists of calculating concentrations at successive time intervals Δt using eq.(8) and then the corresponding mass thickness from eq. (10,11). The concentration profile is obtained by plotting atomic-or weight-concentrations as a function of the integrated mass thickness given by eq. (12). To convert the mass thickness into depth it is necessary to divide the mass thickness $\Delta\mu_i$ by the density d_{AB_i} measured at the i^{th} time interval and to sum up :

$$z(n\Delta t) = \sum_{i=1}^{n} \frac{\Delta\mu_i(A\text{-}B, \Delta t)}{d_{AB_i}} \qquad (13)$$

In many cases it is not necessary to convert the mass thickness into depth to grasp the peculiarities of the profile. If it is, the knowledge of the density as a function of composition is required. Two cases have to be considered : (i) if the profile reveals compounds whose density is known there is no problem for the depth calibration ; (ii) if no density measurement is available interpolation between two known compounds most often gives a good approximation.

Attention is drawn to the fact that the procedure has the advantage of being independent on the sputtering conditions because the mass thickness is a quantity of matter intrinsic to the sample. Therefore, fluctuations of the ion gun intensity or energy have no incidence on the obtained profile. In our experiments, concentration profiles are directly represented as a function of the mass thickness by using a computer program.

The procedure we have described has been tested on a Cu-Al alloy prepared by intermetallic diffusion of two thin aluminium and copper layers (Fig. 4) ; a copper layer 650 Å thick evaporated on oxidized silicon, covered with a 600 Å thick aluminium layer. The total mass thickness was 74.7 $\mu g/cm^2$. After 40 mn diffusion at 300°C, a compound $Al_{20}Cu_{80}$ (weight concentration) corresponding to γ_2 in the phase diagram has been obtained. This compound is homogeneous in the bulk. At the surface the initial aluminium oxide layer acted as a diffusion barrier which explains the aluminium concentration corresponding to alumina and the absence of copper. Diffusion in silicon was also blocked by the oxide layer. Coefficients Γ_{Al} and Γ_{Cu} have been measured independently and alternatively used to recalculate the initial mass thickness. We obtained in both cases a good agreement with the expected value.

Fields of applications of the STIMS method

Elemental quantitative analysis.

Identification of intermetallic compounds : Intermetallic phase diagrams often are not well known at low temperature. In many cases a simple extrapolation of the phase boundaries determined at high temperature is considered. A direct approach to the problem has been proposed by preparing thin layer diffusion couples at low temperature (Tarento, 1982). An example is given in Fig. 5. A thin aluminium film is deposited onto a single copper crystal carefully polished and cleaned. After annealing at 285°C for 2 h 45 mn in-depth analysis was achieved by STIMS.

We are interested for the moment in the composition of the phase diagram not in the in-depth profile that will be discussed further. The diffusion profile exhibits 6 successive plateaus in the aluminium concentration range 0.5 - 0.2 which correspond to the formation of compounds. After a calibration of coefficient $k_{Al\text{-}Cu}$ with a known

Figure 4

Representation of Al and Cu concentrations as a function of mass thickness after alloying two aluminium and copper layers. The two curves have been obtained independently : the upper one after calibration of Γ_{Al} (see text) the lower after calibration of Γ_{Cu}. The accordance with the theoretical value of 74.7 µg/cm² is satisfactory.

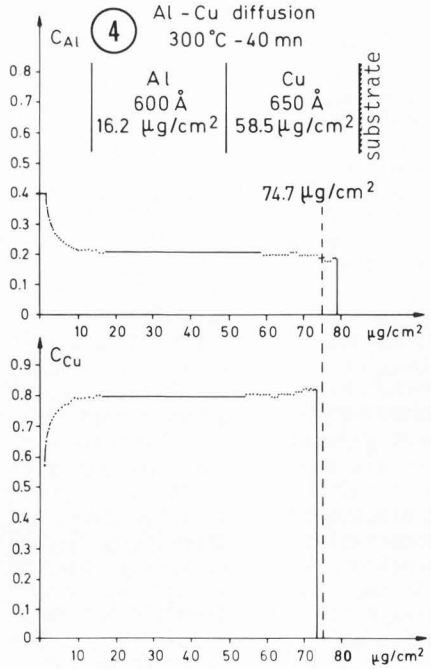

Figure 5

Identification of Al-Cu compounds formed by diffusion at low temperature. Aluminium concentration is plotted versus mass thickness. Hatched areas correspond to the domains of stability of the phases known at high temperature. The total inter-diffusion thickness is about 6000 Å.

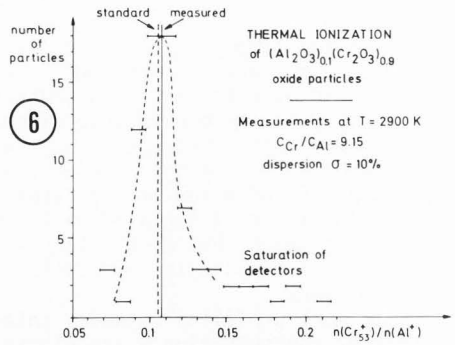

Figure 6

$(Al_2O_3)_{0.1}$ $(Cr_2O_3)_{0.9}$ oxide particle analysis. Histogram of the number of particles versus Cr/Al intensity ratio. Deviation from the standard value of 0.105 is due to statistical fluctuations on the left of the peak and detector saturation on the right.

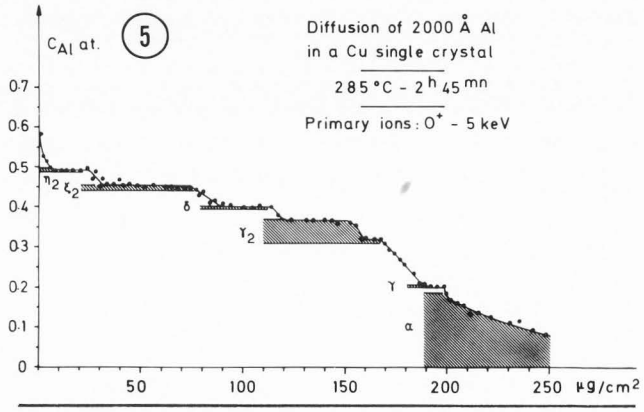

homogeneous Al-Cu alloy we were able to determine the composition of these compounds with accuracy. Aluminium concentrations are indicated in table 2 with the proposed compounds.

The Al-Cu phase diagram is well-known for its complexity to such an extent that it is still a matter of controversy. At low temperature some of the detected compounds were unknown ($Cu_{11}Al_9$ and $Cu_{15}Al_4$ for example) whereas there was a great confusion regarding the existence and composition of others. So, for the three following compounds $Cu_{30}Al_{20}$, $Cu_{32}Al_{19}$ and Cu_9Al_4 it is noted in the literature (Hansen, 1958) : "These three types of structure are so closely related that no two-phase region can be formed between them". Our experiment clearly demonstrates the existence of these three types of compounds and their distinct spatial nucleation without any doubt.

Dust particle analysis : As was suggested by Castaing the method is quite valuable for analyzing dust particles of size between 0.1 and 10 µm just by letting them fall into the cell. The experiment was achieved by thermal ionization with $(Al_2O_3)_{0.1}$-$(Cr_2O_3)_{0.9}$ composite crystals prepared by sintering at 1550° C for 24 hours. The melting point of this solution is about 2300°C. The size of the grains controlled by X-ray diffraction was between 0.1 and 1 µm. A histogram of the number of grains as a function of the signal ratio $n(Cr^+)/n(Al^+)$ is represented in Fig. 6. A peak, whose maximum at 0.108 is close to the expected value 0.105 (standard value), is observed with a rather large dispersion $\sigma \sim 10$ %. The origin of this dispersion is due to the statistical fluctuation of the less intense chromium signal in small grains whereas in large grains it comes from the saturation of the detector receiving the most intense aluminium signal.

An Olivine of composition $SiO_4Mg_xFe_yCa_{0,02}$ was also studied under the same conditions. As in the previous case a peak was obtained for the thermal ionization signal ratio Fe^+/Mg^+ with a comparable dispersion, from which we deduced the concentration ratio x/y = 0.12 ± 0.02. A study of this sample with the electron microprobe gave a similar result but with a better accuracy x/y = 0.113 ± 0.004.

These two examples demonstrate the capability of the thermal ionization method in this important

TABLE 2 *Al-Cu phase diagram at low temperature (285°C)*

C_{Al} (at %)	50	45	40	37.5	31	21
Compound	CuAl	$Cu_{11}Al_9$	$Cu_{30}Al_{20}$	$Cu_{32}Al_{19}$	Cu_9Al_4	$Cu_{15}Al_4$

field of dust grains analysis. However any of this application would require a special attention to specific problems such as :

(i) Contamination of the cell : the liquid film formed by the melting and spreading of a grain at the contact of a cell wall may diffuse in the metal and form very stable compounds, causing memory effects prejudicial to analysis. Contamination of the cell is specific to certain elements. For example aluminium is chemically very active with a tungsten cell. Tantalum seems to be more appropriate for this type of experiment.

(ii) Fractional distillation : some elements evaporate more rapidly than others. As a result quantitation may be disturbed due to the presence of openings in the cell. To reduce this effect it is convenient to use a large cell with very small openings and to let the grains fall far away from these openings.

(iii) Saturation of detectors : in our instrument, we have used channeltrons as detectors for multicollection purposes on account of their small size but they have the disadvantage of being saturated very rapidly ; saturation effects are discernible above 30,000 c/s. Let us consider a particle of 1 μm^3 of volume that contains about 10^{11} atoms. For average thermal ionization yields of 10^{-5} - 10^{-6} this leads to a burst of several hundreds of thousands ions arriving on the detector in a time of a few tenths of second. The saturation of the detector is not surprising in these conditions (see Fig. 6). Dinode electron multipliers should be better for this type of analysis but, in any case, the maximum volume acceptable is a few μm^3.

Behaviour of solid surfaces under ion bombardment.

Many parameters have an influence on the quality of ion erosion. Some of them are characteristic of the sample (nature, structure, roughness, preparation of the surface, ...) others of the ion gun (nature, intensity, energy of ions) still others of the ion-surface interaction conditions (incidence angle, ion density, sputtering yield, ...).

Most often, the ion sputtering technique is carried out in surface analysis apparatus, under fixed conditions in such a manner that experimenters have no possibility to adapt this technique for the best of their analytical problem. As a result, the reader is overwhelmed with a superabundant literature from which it is difficult to extract the most relevant information. Fortunately recent comprehensive review papers (Navinsek, 1977, Betz, 1980, Magee et al. 1982, Hauffe, 1982) cast some light on the main features relative to the ion bombardment on solid surfaces. Our contribution in this field, using the STIMS method, is still too recent for offering a general view of the subject. Emphasis will be placed on some features illustrated by typical examples.

Unnannealed microcrystalline vapor deposited layers : a typical depth profile of a vapor deposited aluminium layer (250 Å) on a single crystal copper substrate is shown in Fig. 7. Erosion was achieved with Ar^+ ions of 5 keV energy. It is clear that in-depth resolution is very poor in this experiment. The examination of the surface after bombardment in a scanning electron microscope reveals the presence of cones whose height is an appreciable part of the layer thickness. Such a topography which has often been reported (Navinsek, 1977) is characteristic of unannealed vapor deposited layers. The only interesting point in the curve of Fig. 7 is the Al^+ signal increases at the onset of erosion. This variation is that typical of the presence of an oxide layer whose thickness is about 30 Å in this case.

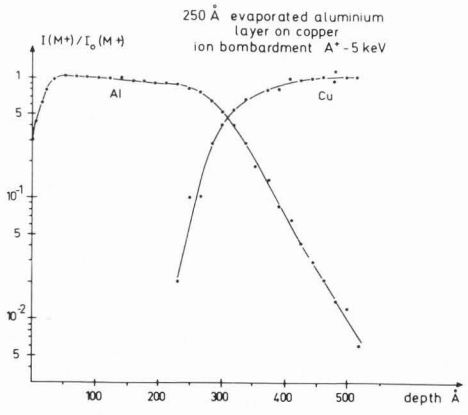

Figure 7

In-depth analysis of a 250 Å unannealed Al evaporated layer on a copper substrate. Ion bombardment by Ar^+ of 5 keV. Al^+ and Cu^+ intensities are normalized to their respective maximum. The increase of the Al^+ signal at the onset of the bombardment is due to the removal of the surface oxide layer.

In-depth analysis under these conditions is obviously of little interest. An embedded layer of a few atomic layers would appear completely diluted in such a profile. So we have to understand the origin of the cones responsible for the bad resolution and look for better sputtering conditions.

A nickel/chromium sandwich multilayer sample composed of 9 successive layers representing about 5000 Å of total thickness has been bombarded by A^+ ions of 4 and 2 keV energy respectively on two distinct regions. The experimental procedure is that described in section on in-depth analysis. After calibration of the relative nickel/chromium ionization coefficient and measurements of Γ_{Ni} and Γ_{Cr}, we plotted nickel and chromium concentrations as a function of depth by introducing the respective densities of the two metals. If erosion were perfect we should have 0 and 1 alternatively for the respective concentrations. The topography created by erosion produces an interpenetration of Ni/Cr layers. So concentrations at depth z represent the fraction areas of the two elements. Figure 8 shows the variation of the apparent chromium concentration as a function of depth in both cases (Ni concentration is just the complementary). Before comparing the two curves let us point out that each experiment lasted 3000 seconds which corresponds to 3000 measurements for each element. It results that erosion velocity was about 1 1/2 Å per second.

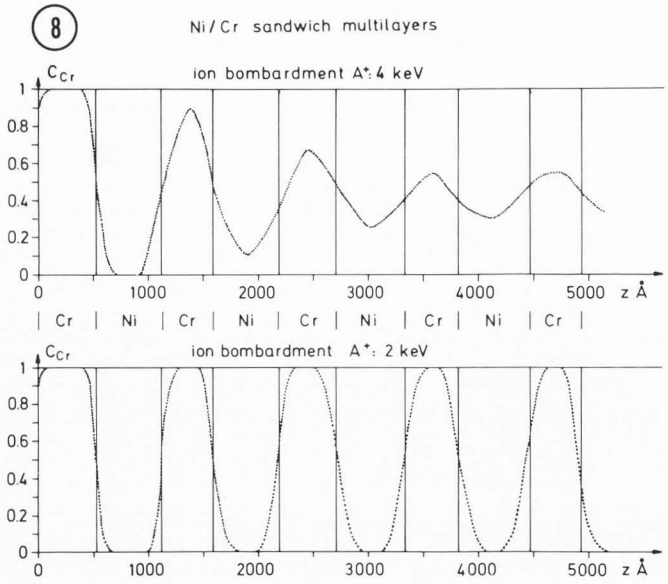

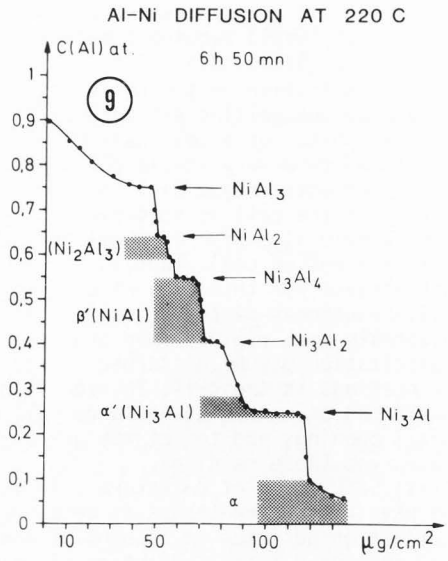

Figure 8

In-depth analysis of Ni/Cr sandwich layers : chromium concentration versus depth z (Ni concentration is the complementary). The upper curve has been obtained with Ar^+ ion bombardment of 4 keV energy, the lower one with 2 keV energy. Vertical lines delimit the successive layers whose thickness has been calculated using the mass thickness procedure (see text).

Figure 9

Al-Ni diffusion diagram obtained at 220°C. Aluminium concentration plotted versus mass thickness. The total thickness is about 4000 Å. Compounds identified : $NiAl_3$, $NiAl_2$, Ni_2Al_3, Ni_3Al_4, Ni_3Al_2, Ni_3Al. Hatched areas are relative to the domains of stability of the phases as they are determined at higher temperature (Tarento, 1982).

The difference in the in-depth resolution is flagrant from the comparison of the two curves. Under a 4 keV ion bombardment resolution is diminishing very rapidly. There is a complete mixing of layers beyond the first two ones. This situation is similar to that in Figure 7. Under a 2 keV ion bombardment, Ni and Cr concentrations reach unity even in the deepest embedded layers on half of the thickness at least. As there is a complete separation between Ni and Cr signals we were able, in that case, to recalculate the thickness of the successive layers just by integrating independently each signal. It appears that Cr and Ni layers are respectively about 500 Å and 600 Å thick with a slight dispersion of ±30 Å that could come from our experimental procedure.

This influence of the ion energy on the depth resolution deserves a special attention. There are two major causes of the degradation of resolution with depth : the original surface roughness (Hofmann et al., 1977) and the crystalline transparency (Blaise and Castaing, 1978, Coudray et al., 1982). The incidence angle dependence of the sputtering yield $S(\theta) \sim S_0/\cos\theta$ (Sigmund, 1972) (θ being measured to the surface normal) leads to emphasize the relief of a rough surface. On the other hand the crystalline dependence of the sputtering yield causes the erosion velocity to vary in large proportions (by a factor of 2 on the average) from one grain to another in a polycrystalline sample (as vapor deposited layers are), from which a stepped relief is created. Combination of these two effects results in the formation of cones.

In our two experiments the initial roughness was the same. But $S(\theta)$ dependence is less pronounced at low energy than expected from the theory as it was observed by Oechsner (1975) (see appendix). On the other side, transparency effects are also less pronounced at low energy since collision cascades are developing closer to the surface (see appendix). Combination of these two propitious circumstances makes in-depth resolution better at low energy. What is surprising in our experiments is the rapid transition from a very bad situation at 4 keV to a better one at 2 keV. We are going to study this problem in detail in the near future by varying step by step the ion energy from 5 keV to a few hundreds eV.

Annealed microcrystalline vapor deposited layers : The ion erosion of annealed layers was studied in the course of an extensive work on thin layer intermetallic diffusion (Tarento, 1982). The general procedure consists of evaporating a thin layer of a few thousands Å of metal A onto a single crystal substrate B. After diffusion, in-depth analysis must reveal the intermetallic compounds formed. An example has been given in Fig. 5 already. But now, our ambition was to detect these compounds

just after their nucleation at the first stage of their growth in order to determine germination compositions, diffusion coefficients, activation energies, growth kinetics. So we were expecting very thin layers distributed in successive strata parallel to the surface with sudden composition changes from one compound to another. Extremely good in-depth resolution was required for such an analysis and we could fear the worst from the results obtained on unannealed layers. Fortunately the situation seems quite different in annealed layers. An example is given in Figure 9 for the Al-Ni couple where the aluminium concentration has been plotted as a function of the mass thickness. The total diffusion profile is about 4000 Å. Annealing temperature was 220°C for 6 h 50 mn. In-depth analysis was carried out with 4 keV A^+ ion energy. A monotonous decrease of the Al concentration is first observed at the surface, followed by a cascade of plateaus till the α(Al, Ni) solid solution. The initial Al concentration decrease corresponds to a rapid intergranular nickel diffusion in the polycrystalline aluminium layer. Each plateau is a compound. We have found 6 compounds : $NiAl_3$, $NiAl_2$, Ni_2Al_3, Ni_3Al_4, Ni_3Al_2, Ni_3Al. Except for the first one they were unknown at low temperature. When the diffusion time is increased or the temperature raised no new compound appears. We have just observed a growing of these ones. In the present state of diffusion their respective thickness was varying from ∿ 30-50 Å ($NiAl_2$ and Ni_2Al_3) to 300 Å (Ni_3Al).

In these experiments, it is quite remarkable to detect such thin layers embedded so deeply (at about 2000 Å) under a polycrystalline layer. It demonstrates the ion erosion of an annealed layer is less sensitive to bombarding conditions than an unannealed one. Therefore, the problem of in-depth resolution appears to be extremely complex. The interpretation we gave in the previous section is not in contradiction with what we obtained here, but it requires one to consider the specificity of the sample to be eroded : the annealing of a vapor deposited layer changes the original topography thoroughly by recrystallisation. This is probably why erosion becomes more uniform. Examination of the eroded surface in a scanning electron microscope reveals no pronounced relief : at a magnification of 4.10^4 a waved surface is faintly visible with a periodicity of about 1000 Å and an amplitude not measurable.

Looking carefully at the depth resolution between two successive plateaus, the composition change requires a few atomic layers in general which is quite good. However between Ni_3Al_2 and Ni_3Al (Fig. 9) the transition is longer. This can be ascribed to an heterogeneous germination of these two compounds on both sides of the original Al/Ni interface.

From a metallurgical point of view these experiments allow us to show the non stoichiometric germination of compounds (for example there is a depletion of 2 at % of Al concentration at Ni_3Al germination) ; to identify new compounds unknown at low temperature (for example $NiAl_2$, Ni_2Al_3, Ni_3Al_4, Ni_3Al_2, Ni_3Al) ; to measure diffusion coefficients and activation energies.

It is interesting to note that most of the new compounds correspond to the phase boundaries of the domains of stability determined at higher temperatures. For the diffusion coefficients they are of the order of 10^{-16} cm^2/s at 220°C ; that is several orders of magnitude higher than expected from the extrapolation of high temperature measurements.

To conclude this section, we would suggest that intermetallic diffusion at low temperature could be used for preparing standards of well defined compositions as those presented in Fig. 9, to quantify Auger Spectroscopy for example.

Metal amorphous compounds : In an amorphous structure sputtering effects relative to crystalline texture are vanishing. So we can expect the erosion is less sensitive to the bombarding conditions ; the only ultimate limitation being the depth fluctuations due to the random character of sputtering.

Metal amorphous layers have been prepared by cathodic sputtering of CuTi and Cu_3Ti (Tarento, 1982). A 20 µm thick layer of CuTi was first deposited on a silicon substrate, then a 2000 Å thick Cu_3Ti layer. The amorphous character was controlled before and after in-depth analysis. In-depth analysis was carried out with 4 keV energy A^+ ions. The Cu/Ti concentration ratio is plotted as a function of depth in Figure 10. The step

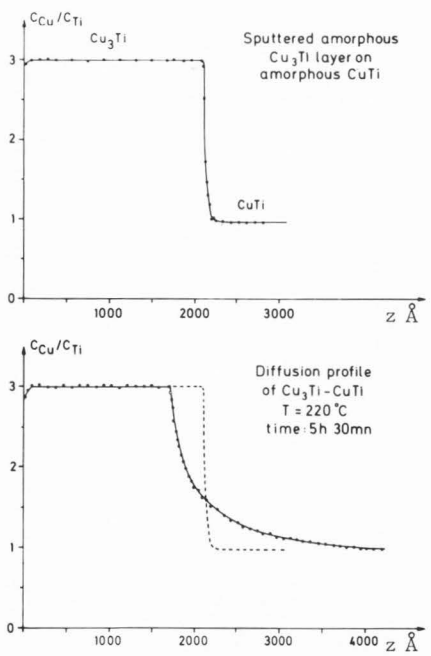

Figure 10

In-depth analysis of CuTi, Cu_3Ti amorphous compounds. Bombardment by A^+ ions of 4 keV energy. Copper to titanium concentration ratio plotted versus depth. The upper curve has been obtained before diffusion, the lower one after diffusion at 220°C (Tarento, 1982).

observed between the two plateaus is less than 60 Å thick. Compared to the erosion of unannealed polycrystalline layer (Fig. 7) this is extremely good. This result confirms the absence of crystallinity is determinant for the quality of erosion. The same sample was studied after diffusion at 220°C for 5h 30 min. The in-depth profile is shown in Fig. 10. The diffusion profile obtained is not of a usual shape : it is characterized by an assymmetry which reminds us of a percolation of copper from the Cu_3Ti layer through the underlying CuTi layer.

Ion bombardment induced surface compositional changes : Surface compositional changes induced by ion bombardment have been extensively investigated recently by methods analyzing either the remaining surface composition as Auger Spectroscopy (Ho et al., 1976, 1977, Betz, 1980, Betz et al., 1981) or the composition of the sputtered matter as SIMS (Toyokawa et al, 1981). In fact a comprehensive view of the problem would require a correlated investigation of surface and sputtered matter compositions since these two compositions are complementary. This is what we have done by associating Auger Spectroscopy with STIMS (manuscript submitted).

Let us consider a binary compound A-B whose surface concentration ratio is $(C_A/C_B)_{surface}(z)$. At depth z, we have :

$$\left(\frac{C_A}{C_B}\right)_{surface}(z) = \nu_{AB}\left(\frac{C_A}{C_B}\right)_{sputtered}(z) \qquad (14)$$

Such a relation has often been proposed for relating surface and bulk concentrations under steady state sputtering conditions. In fact eq. (14) is valid at any stage of erosion, in particular during the transient regime of the compositional change. Coefficient ν_{AB} is one of the fundamental parameters of the process of composition change. It has been measured in the case of Zn-Cu alloys (manuscript submitted) and found to be constant over a large concentration range (up to 33 at % of Zn) : $\nu_{ZnCu} = 0.36$. Including this value in eq. (14) we were able to recalculate the erosion time dependence of the surface composition in a $Zn_{0.67}Cu_{0.33}$ alloy from measurements of the sputtered matter composition by STIMS (Fig. 11). In this figure, zinc and copper concentrations have been plotted as a function of the sputter time. Open circles and crosses represent the time evolution of the sputtered matter composition. Dashed curves are the surface compositions recalculated from eq. (14). It is noticed that the sputtered matter composition equals the bulk composition $Zn_{0.67}Cu_{0.33}$ when the sputtering steady state is reached ; the original composition at t = 0 being different. Surface composition under the sputtering steady state exhibits a depletion of Zn ($C^s_{Zn} = 0.15$) and an excess of copper ($C^s_{Cu} = 0.85$) with respect to the bulk composition. In the case of these Zn-Cu alloys the composition change is particularly strong, about 60 % of the bulk Zn concentration. The original surface composition appears slightly enriched in zinc (∿ 0.45) compared to the bulk (0.33). This calculation of the surface composition is in good agreement with AES measurements. Measurement of coefficient ν was also used for the benefit of Auger spectroscopy for determining the real alloy composition (manuscript submitted).

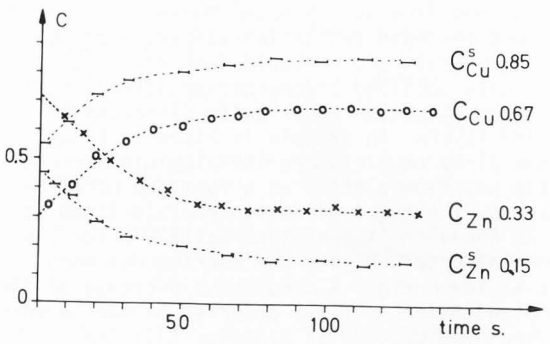

Figure 11

Time evolution as measured by STIMS of Zn and Cu concentrations in the sputtered matter from a $Zn_{0.67}Cu_{0.33}$ alloy bombarded with 4 keV energy A^+ ions. Open circles and crosses are Zn and Cu concentrations in the sputtered matter. Dashed curves are surface concentrations calculated from eq. (14) with $\nu_{ZnCu} = 0.36$.

Conclusion

Sputtered thermal ion mass spectrometry is a new quantitative method of solid analysis devoid of matrix effects. Its sensitivity is comparable to or even better than that of electron spectroscopy methods. Unfortunately some major elements such as oxygen, carbon or boron are not yet detectable. But these difficulties can hopefully be overcome by using less chemically active materials than Ta or W for the hot cell.

An important application is the quantitative elemental analysis of compounds produced in thin layers, for example, or dust particle of medium size 0.1 to 10 µm.

Due to its quantitativeness it can be used for the study of ion bombardment in-depth resolution in various solids and under various conditions and the study of ion bombardment induced surface compositional changes. In-depth analysis constitutes its major field of application.

Acknowledgements

We are grateful to Dr. Jo Geller from JEOL. USA for providing us Ni/Cr sandwich layers.

Appendix

Remarks on the incidence angle and crystalline structures dependences of the sputtering yield.

1) For $\theta \lesssim 70°$ the angular dependence of the sputtering yield is predicted to vary as $S(\theta) = S_o \cos\theta^{-5/2}$ from Sigmund's theory (Oechsner, 1975) ; S_o being the sputtering yield at normal

incidence, θ the incidence angle to the surface normal. Experimentally a $\cos \theta^{-n}$ law is observed with $n \gtrsim 1$ at high energy ($\gtrsim$ 20 keV) (Blaise, 1978) whereas at low energies $n << 1$ (1 keV for example (Oechsner, 1975)).

Let r be the radius of the core of the collision cascades considered as the emissive source of sputtered atoms. If the core is located at depth z below the surface, such as $z >> r$, that is at high energy, the escape probability of an atom will be proportional to λ/z where λ is the mean free path. Therefore a $\cos \theta^{-n}$ law with $n \sim 1$ will be observed for the sputtering yield angular dependence : the higher the angle θ, the closer to the surface the emission core.

Now, if energy is low enough such as $z << r$ whatever the incidence angle is, the above argument is no longer valid. The core of the collision cascades intersecting the surface, becomes the direct emission source of sputtered atoms, almost independent of the primary ion incident angle. Therefore it is normal to observe an attenuation of the angular dependence of the sputtering yield ($n << 1$) at low energy ; and consequently a reduction of effects induced by the original surface roughness.

2) About the crystalline dependence of the sputtering yield it is well known (Blaise, 1978, Coudray et al., 1982) that sputtering with ions of a few keV energy is initiated by the number of primary collisions occurring in the first 3 or 4 atomic layers, most of the sputtered atoms coming from the top layer. Transparency effects are related to the probability of producing primary collisions in these 3 or 4 atomic layers, according to the relative orientation of the primary beam with respect to the crystalline rows. As the primary energy is lowered, primary collisions involved in the sputtering process must be located closer to the surface ; that is in the first or in the second layer, which reduces transparency effects in proportion. At the limit if energy was low enough we could imagine that only primary collisions in the top layer could initiate microcascades leading to the ejection of atoms from this layer. In that case transparency effects would be completely suppressed.

References

Betz G. (1980), "Alloy sputtering". Surface Science 92, 283-309.

Betz G., Dudonis J., Braun P. (1981), "Surface enrichment in Ag-Au-Pd alloys under ion bombardment."Surface Science 104, L185-L188.

Blaise G. (1978). "Fundamental aspects of ion microanalysis. Material characterization using ion beam. NATO Advanced study institute series. Series B Physics 28, 143-238.

Blaise G., Bernheim M. (1975), "Adsorption of gases studied by secondary ion emission mass spectrometry". Surface Science 47, 324-343.

Blaise G., Castaing R. (1977). "Analyse des surfaces par ionisation thermique des produits de pulvérisation cathodique". C.R. Acad. Sci. Paris, série B, 284, 449-452.

Blaise G., Castaing R. (1978). "Présentation d'une méthode de microanalyse des solides fondée sur l'ionisation thermique des produits de pulvérisation". J. Microsc. Spectrosc. Electron. 3, 439-446.

Blaise G., Castaing R., Quettier R. (1984). "Méthode d'analyse fondée sur l'ionisation par electrons des produits de pulvérisation thermalisés. Journal de Physique, Colloque C2, supplément au n° 2, 45, 125-127.

Castaing R., Blaise G. (1980). "Analysis of solid surfaces by thermal ionization of sputtered particles". 8th Intern. Conf. on X-Ray optics and Microanalysis, Boston - R. Beaman, R.E. Ogilvie, D.B. Wittry (Eds). Pendell Publ. Co., Midland, Michigan, 3-7.

Castaing R., Slodzian G. (1962). "Microanalyse par émission ionique secondaire". J. Microscopie 1, 395-410.

Couchouron M. (1983). "Ionisation thermique de surface des produits de pulvérisation - Possibilités analytiques". Thèse de Doctorat d'Etat. Université Paris XIII - 93430 Villetaneuse, France.

Coudray C., Bernheim M., Slodzian G. (1982). "Effets d'ombrage observés lors de la rétrodiffusion d'ions lents sur un cristal métallique : simulation et expériences". J. Microsc. Spectrosc. Electron. 7, 459-475.

Eloy J.F. (1980). "Recent developments in laser microprobe mass spectrometry." 5th International Symposium "High purity materials in science and technology". Proceedings II : characterization - Akademic der Wissenschaften der DDR Zentralinstitut für köperphysik un Werskstofforschung. Dresden DDR, 96-110.

Hansen M. (1958). "Constitution of binary alloys." Second edition - Mc Graw Hill, 118-121.

Harrison W.W., Magee C.W. (1974). "Cathode ion source for solids mass spectrometry". Anal. Chem. 46, 461-464.

Hauffe W. (1982) "Surface topography development during SIMS investigation and using it to get additional information on polycrystalline and heterogeneous solids." Secondary Ion Mass Spectrometry, SIMS III. Springer series in Chemical Physics 19. A. Benninghoven, J. Giber, J. Laszlo, M. Riedel, H.W. Werner (Eds), Springer-Verlag, N.Y. 206-210.

Heinrich K.F.J. (1981). "Electron beam X-ray microanalysis". Van Nostrand Reinhold, NY, 10, 255-301.

Hennequin J.F., Couchouron M. (1979). "Application de l'ionisation de surface à l'analyse des produits de pulvérisation". J. Microsc. Spectrosc. Electron. 4, 513-519.

Ho P.S., Lewis J.E., Wildenau H.S., Howard J.K. (1976). "Auger study of preferred sputtering on binary alloy surfaces". Surface Science 57, 393-405.

Ho P.S., Lewis J.E., Howard J.K. (1977). "Auger study of preferred sputtering on Ag-Au alloy surfaces." J. Vac. Sci. Technol. 14, n° 1, 322-325.

Hofmann S., Erlewein J., Zalar A. (1977). "Depth resolution and surface roughness effects in sputter profiling of NiCr multilayer sandwich samples using Auger electron spectroscopy". Thin Solid Films, 43, 275-283.

Magee C.W., Honig R.E., Evans C.A.Jr. (1982). "Depth profiling by SIMS : depth resolution dynamic range and sensitivity. Secondary Ion Mass Spectrometry SIMS III. Springer Series in Chemical Physics 19. A. Benninghoven, J. Giber, J. Laszlo, M. Riedel, H.W. Werner (Eds). Springer Verlag, N.Y. 172-185.

Marcyk G.T., Streetman B.G. (1976). "Boron impurity profile tailoring in silicon by ion implantation and measurement by glow discharge optical spectroscopy." J. Electrochim. Soc., 123, 1388-1391.
Navinsek B. (1977). "Sputtering - Surface changes induced by ion bombardment". Progress in Surface Science - Pergamon Press, Great-Britain, 7, 49-70.
Oechsner H. (1975). "Sputtering. A review of some recent experimental and theoretical aspects." Appl. Phys. 8, 185-198.
Oechsner H., Ruhe W., Stumpe E. (1979). "Comparative SNMS and SIMS studies of oxidized Ce and Gd." Surface Science, 85, 289-301.
Sigmund P. (1972). "Collision theory of displacement damage, ion ranges and sputtering." Rev. Roum. Phys. 17, 823-870, 969-1000, 1079-1106.
Slodzian G. (1964). "Etude d'une méthode d'analyse locale chimique et isotopique utilisant l'émission ionique secondaire." Ann. Phys. Paris 9-10, 591-648.
Slodzian G. (1975). "Some problems encountered in secondary ion emission applied to elementary analysis." Surface Science 48, 161-186.
Tarento R. (1982). "Etude de la diffusion en couches minces dans les matériaux cristallins et amorphes par thermo-ionisation." Thèse de 3ème cycle, Université Paris-Sud, 91405 Orsay, France.
Toyokawa F., Furuya K., Kikuchi T. (1981). "A static SIMS study on preferential sputtering on copper-nickel alloy surface." Surface Science, 110, 329-338.

Discussion with Reviewers

W. Katz : The acronym STIMS is not really correct since this method employs electron impact as well as thermal ionization.
Author : The originality of our method is the thermalization of the sputtered matter which opens the way to a quantitative analysis procedure. This is why we have chosen this acronym. The ionization process used is of little importance. Processes other than those mentioned in the text could be used (ionization by a laser or a metastable beam for example).

R. Gijbels : I assume from the text that for dust particle analysis no electron impact ionization is used, only thermal ionization : is it correct ? How many submicron size grains are introduced into the hot cell, and how is this done in practice ?
Author : This experiment on dust particles was carried out by using thermal ionization at a time when the electron impact ionization device was not yet developed. Of course there is no objection to use an electron impact ionization in these experiments. Dust particles were deposited on an appropriate grid place above one of the openings of the cell and maintained by a long rod. A knock on the rod produced a vibration that was sufficient to separate the particles from the grid and let them fall into the cell.

R. Gijbels : How was the amorphous character of the metal layers controlled before and after in-depth analysis ?
Author : The amorphous character was proved by the observation of the X-rays characteristic diffusion annulus.

R. Gijbels : Does the author have any metal in mind which has a sufficiently high melting point, but which is less reactive than Ta or W for use as a hot cell ?
Author : The only other metal having a sufficiently high melting point is Re but it is more reactive than Ta or W. So I think that the solution is in the use of compounds such as carbides or borides.

R. Gijbels : Is it not more usual to observe a decrease in the Al^+ signal (Fig. 7) from an oxidized, argon bombarded Al metal surface, as a function of depth ?
W. Katz: My major concern is with the statement that this method is free of matrix effects. The profile of Al (Fig. 7) shows clearly oxygen enhancement of the surface as is noted in all SIMS experiments.
Author : In SIMS experiments the metal ion intensity M^+ is very sensitive to the presence of oxygen: there is a strong enhancement of the ionization coefficient (this is the chemical effect). For example, in SIMS the Al^+ signal emitted by Al_2O_3 is about 100 times higher than in pure aluminum when bombarding with argon.

As the surface of a metal is always oxidized it is usual to observe a decrease of M^+ by several orders of magnitude during the erosion of the natural oxidized layer by argon ions, before stabilization.

In our case we have no chemical enhancement effect due to oxygen. For example, when bombarding Al_2O_3 and Al with an argon beam we observe an intensity ratio of the two Al^+ signals $\sim$ 0.2-0.6. This ratio is the product of the aluminum concentration in the oxide 0.4 by the ratio of the two sputtering yields that is :

$$0.4\ S_{Al_2O_3}/S_{Al} \sim 0.2\text{-}0.6$$

This is the variation of S_{Al} with the crystalline orientation which causes the variation from 0.2 to 0.6 of the intensity ratio.

In the profile presented in Fig. 7 the depletion at the surface of the Al^+ signal corresponds to the values indicated above. It is due to the presence of a very thin oxide layer.

All our experiments demonstrated that under state sputtering conditions ; there are no matrix effects as those observed in SIMS ; that is matrix effects related to the sample chemical composition. In our method the ionization coefficients could be affected by the sample composition if the cell was contaminated by the sputtered matter itself. This is why it is necessary to operate at a very high temperature to prevent the cell from contamination.